ACS APPLIED NANO MATERIALS
Cite This: ACS Appl. Nano Mater. 2018, 1, 6904−6911
Article
www.acsanm.org

Thermal Stability of Alumina-Overcoated Au_{25} Clusters for Catalysis

V. Sudheeshkumar,[†] Andrew Lushington,[‡,§] Xueliang Sun,[‡] and Robert W. J. Scott*[,†]

[†]Department of Chemistry, University of Saskatchewan, 110 Science Place, Saskatoon, Saskatchewan S7N 5C9, Canada
[‡]Department of Mechanical and Materials Engineering, University of Western Ontario, London, Ontario N6A 5B9, Canada

Supporting Information

ABSTRACT: One of the prevalent difficulties in using supported gold (Au) cluster or nanoparticle materials for catalytic applications is the ease at which such systems sinter at even moderate temperatures and conditions. Herein we demonstrate a stabilization strategy involving atomic-layer-deposition (ALD) of alumina overlayers onto supported Au clusters, which greatly alleviates high-temperature sintering. Control over both the number of cycles (5, 10, and 20) of alumina deposition over Au_{25} clusters and the surface chemistry of the clusters themselves was found to be important for optimal stabilization. Transmission electron microscopy and extended X-ray absorption fine structure analyses showed that Au_{25} clusters using 11-mercaptoundecanoic acid stabilizers with 20 cycles of alumina overcoating via ALD showed remarkable thermal stability, with particle sizes growing only slightly to ca. 2.5 nm after calcination at 650 °C. However, such stabilization does come with a cost; at moderate temperatures, 10-cycle alumina-coated catalysts showed better catalytic activity for a 4-nitrophenol reduction reaction than 20-cycle alumina-coated catalysts, which is likely because of increased mass-transfer resistance associated with the protective shell.

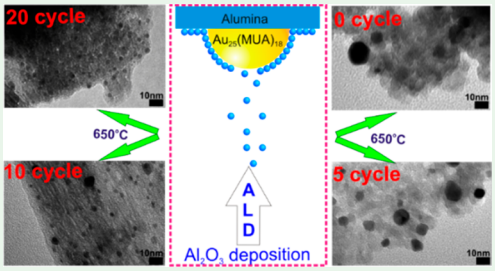

KEYWORDS: *Au_{25} clusters, sintering, atomic layer deposition, extended X-ray absorption fine structure, catalysis, reductions*

INTRODUCTION

Gold (Au) catalysts supported on reducible and nonreducible metal oxides have been studied for many reactions, including low-temperature CO oxidation, partial oxidation of hydrocarbons, and reduction of nitrogen oxides.[1−3] One important conclusion that has arisen from previous studies with Au catalysts is that Au nanoparticles have remarkable size-dependent catalytic activity, with Au particles below 4 nm having strong catalytic activity and particles greater than 6 nm being nearly inactive.[4−6] Thiol-stabilized Au clusters with sizes in the 1 nm range (such as $[Au_{25}(SR)_{18}]$) have been shown to be model catalysts for many oxidation and reduction reactions at moderate temperatures.[7−9] Such clusters are ideal model catalysts because they can be prepared with high purity and monodispersity, thus allowing for precise structure−property relationships to be obtained. However, Au clusters/nanoparticles rapidly sinter under reaction conditions and/or thermal activation treatment and form larger particles.[10] Because of this limitation, commercialization of supported Au catalysts has been restricted to low-temperature applications.

Several methods, such as chemical vapor deposition (CVD),[11] grafting of amines onto nanoparticles,[12] dendrimer encapsulation,[13] and encapsulation by the sol−gel method,[14,15] have been reported to help alleviate sintering of metal clusters and nanoparticles. Previously, we documented that silica-encapsulated $Au_{25}(MUA)_{18}$ (MUA = 11-mercaptoundecanoic acid) clusters showed significant sinter resistance up to 650 °C and that the resulting catalysts still showed good activity and recyclability for styrene epoxidation reactions.[15] However, mass-transfer issues associated with the protective silica shell were problematic. CVD is a thin-film deposition technique involving the reaction of gas-phase precursors at or near the vicinity of the substrate.[16] Atomic layer deposition (ALD) is a self-limiting, multistep gas-phase CVD technique that provides a unique method for depositing ultrathin films on surfaces. In the ALD process, growth progresses layer by layer by applying sequential alternating pulses of gaseous precursors. During each half-cycle, the gas precursor is pulsed into a reaction chamber for a certain time to allow the precursor to react with the substrate, followed by removal of the unreacted precursor. This allows for the fabrication of thin films with precise thickness control at the atomic level, high uniformity, and excellent conformality.[17−22] In contrast to other methods, ALD is a non-line-of-sight technique capable of coating high-surface-area materials in a conformal manner.[18] For example, Ma et al. reported that silica coating by ALD over Au (∼5 nm)/TiO_2 catalysts could enhance the thermal stability of the nanoparticles.[23] Smaller Au particles were successfully coated by ALD of silica, whereas larger particles were noncoated or incompletely coated. Feng et al. reported that 16 cycles of alumina overcoating [one cycle consisting of trimethylaluminum (TMA) exposure followed by water (H_2O) exposure] on palladium (Pd) nanoparticles (1−2 nm) by ALD prevented

Received: September 27, 2018
Accepted: November 8, 2018
Published: November 8, 2018

DOI: 10.1021/acsanm.8b01709
ACS Appl. Nano Mater. 2018, 1, 6904−6911

sintering of the Pd particles after heating to 500 °C for 6 h in an argon flow.[24] In addition, they observed that the catalytic activity for methanol decomposition dropped when over 16 cycles of ALD alumina coatings were used, presumably because of mass-transfer issues. Stair et al. observed that 45 cycles of alumina deposition over Pd/Al_2O_3 were required to maintain the size of the Pd nanoparticles at 2.8 ± 0.46 nm at high temperatures and long reaction times (675 °C for 1700 min).[25]

In this work, the ALD technique was utilized to create protective overlayers of alumina over supported Au_{25} clusters. To probe the critical role of carboxyl groups on the surface of MUA ligands in the ALD process, the thermal stability of alumina-overcoated dodcanethiolate-stabilized Au_{25} clusters was compared with that of alumina-overcoated $Au_{25}(11\text{-MUA})_{18}$ clusters. Transmission electron microscopy (TEM) results showed that tremendous sintering was observed at 650 °C in the absence of carboxylic acid groups, while the $Au_{25}(MUA)_{18}$ system showed dramatically improved stability. Scheme 1 illustrates the stepwise addition of TMA and H_2O to

Scheme 1. Schematic Illustration of Alumina Deposition over $Au_{25}(MUA)_{18}/Al_2O_3$[a]

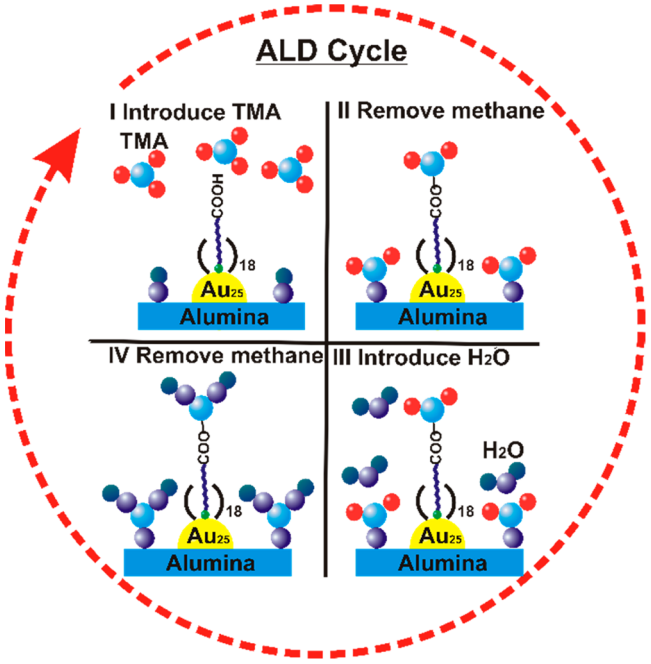

[a]Color scheme: red circles, methyl groups; light-blue circles, Al; dark-purple circles, O; dark-blue circles, H.

the carboxyl groups on the cluster surfaces, which allows for ALD growth to occur over the $Au_{25}(MUA)_{18}$ clusters. The optimal number of ALD layers was also investigated, and the resulting materials before and after calcination at temperatures of up to 650 °C were analyzed by TEM and extended X-ray absorption fine structure (EXAFS) spectroscopy analyses, while the catalytic activity of the clusters was examined via a model nitrophenolate reduction reaction. Catalysts with 20 cycles of alumina overcoating were found to effectively mitigate the sintering of clusters, albeit while introducing mild mass-transfer concerns at moderate calcination temperatures.

MATERIALS AND METHODS

Materials. Hydrogen tetrachloroaurate(III) trihydrate ($HAuCl_4 \cdot 3H_2O$; 99.9% on metal basis, Aldrich), 11-mercaptoundecanoic acid (11-MUA; 95%, Sigma-Aldrich), dodecanethiol (DDT; 98%, Sigma-Aldrich), tetraoctylammonium bromide (TOAB; 98%, Aldrich), sodium borohydride ($NaBH_4$; 98%, EMD), 4-nitrophenol (PNP; 99%, Alfa Aesar), alumina (Al_2O_3; pore size 58 Å, Sigma-Aldrich), and trimethylaluminum (TMA; 98%, Strem) were used as received. Tetrahydrofuran (THF; high purity) was purchased from EMD. Milli-Q water (H_2O) was used for ALD synthesis.

Synthesis of $Au_{25}(MUA)_{18}$ Clusters. $Au_{25}(MUA)_{18}$ clusters were synthesized by using an existing procedure that was published by our group.[26] Briefly, $HAuCl_4 \cdot 3H_2O$ (200 mg) and TOAB (1.2 equiv) were added to 20 mL of THF. The solution was kept stirring until it turned from yellow to orange-red. After the addition of 11-MUA (5 equiv in 5 mL of THF), the solution was stirred until it became colorless. The solution was then cooled using an ice bath, followed by the dropwise addition of ice-cold $NaBH_4$ (4 equiv in 2 mL of H_2O), and the solution was monitored using UV−vis spectroscopy. The addition of $NaBH_4$ was continued until the characteristic UV−vis absorption peaks of the $Au_{25}(MUA)_{18}$ clusters were observed. Larger nanoparticles were then removed by centrifugation at 10000 rpm for 2 min. $Au_{25}(MUA)_{18}$ clusters were precipitated out with further $NaBH_4$ (1.5 equiv in 2 mL of H_2O) addition. The residue was then centrifuged and washed with THF twice, followed by dissolution in H_2O. $Au_{25}(MUA)_{18}$ clusters were precipitated out with a few drops of dilute acetic acid with an approximate pH of 3. The precipitate was washed with H_2O twice and dissolved in THF.

$Au_{25}(MUA)_{18}$ clusters were deposited on alumina by the following procedure: 200 mg of alumina was added to the $Au_{25}(MUA)_{18}$ solution and stirred for 2 h. After stirring, $Au_{25}(MUA)_{18}/Al_2O_3$ catalysts were dried by solvent evaporation.

Synthesis of $Au_{25}(DDT)_{18}$ Clusters. To a solution of $HAuCl_4 \cdot 3H_2O$ (500 mg) in THF (50 mL) were added TOAB (1.2 equiv) and DDT (5 equiv).[27] The resulting solution was stirred until it became clear, followed by the addition of ice-cold $NaBH_4$ (10 equiv in 10 mL of H_2O). The solution was stirred at room temperature for 4 days. The solid was then collected by evaporation of the solvent and washed with an ethanol/H_2O mixture three times, followed by redissolution in THF. The alumina-supported $Au_{25}(DDT)_{18}$ clusters were synthesized in a manner similar to that in the procedure using $Au_{25}(MUA)_{18}$ clusters above.

ALD of Alumina over $Au_{25}(MUA)_{18}/Al_2O_3$ and $Au_{25}(DDT)_{18}/Al_2O_3$. ALD was carried out by the sequential exposure of TMA and deionized H_2O at room temperature. ALD films were deposited using a commercial cross-flow-type hot-wall ALD reactor (Arradiance Gemstar-8) using TMA and Milli-Q deionized H_2O. All precursors were evaporated with an external reservoir held at room temperature. Argon (99.999% Praxair) was used as both carrier and purge gases. Thiolate-protected Au clusters were loaded into a boat and placed in the ALD chamber, which was pumped down to ∼50 mTorr. All depositions were conducted at 60 °C using a 50 ms pulse of TMA and a 50 ms pulse of H_2O separated by a 60 s purge of argon at a flow rate of 20 sccm. Alumina-overcoated samples were prepared using 5, 10, and 20 cycles of TMA/H_2O. For brevity, catalysts prepared by different cycles (5, 10, and 20) of ALD coating are designated as 5c-Al_2O_3/Au(MUA)/Al_2O_3, 10c-Al_2O_3/Au(MUA)/Al_2O_3,, and 20c-Al_2O_3/Au(MUA)/Al_2O_3, respectively, whereas the sample prior to ALD is designated as Au(MUA)/Al_2O_3. The 10c-Al_2O_3/$Au_{25}(DDT)_{18}/Al_2O_3$ catalysts were prepared using 10 cycles of alumina deposition on $Au_{25}(DDT)_{18}/Al_2O_3$. All samples were then dried at 100°C. Further calcinations were carried out at two different temperatures (250 and 650 °C) for 3 h in air.

Characterization. A Varian Cary 50 Bio UV−vis spectrometer was used to collect UV−vis absorption spectra of the $Au_{25}(MUA)_{18}$ clusters. The morphology of the ALD-coated Au_{25}/Al_2O_3 materials was analyzed by a HT7700 transmission electron microscope operating at 100 kV. *ImageJ* software was used to measure the size of 200 particles for particle-size-distribution histograms.[28] EXAFS

DOI: 10.1021/acsanm.8b01709
ACS Appl. Nano Mater. 2018, 1, 6904−6911

spectroscopic analysis was performed on the HXMA beamline 061D-1 (energy range 5−30 keV; resolution 1×10^{-4} $\Delta E/E$) at the Canadian Light Source (CLS). The storage ring electron energy and ring current were 2.9 GeV and 250 mA, respectively. All data were collected in fluorescence mode using a 32-element detector. The energy for the Au L_3-edge (11919 eV) was selected by using a Si(111) double-crystal monochromator with a rhodium-coated 100-nm-long Kirkpatrick−Baez mirror. Higher harmonics were removed by detuning the double-crystal monochromator. Data analysis and EXAFS fitting were carried out using the *Demeter* software package.[29] An amplitude reduction factor of 0.86 was obtained from fitting of the Au foil. The coordination number (CN) of calcined Au cluster samples was determined by keeping this amplitude reduction factor fixed.

Catalytic Activity for PNP Reduction. A total of 2.0 mL of 0.10 mM PNP and 2.0 mg of ALD-coated Au_{25}/Al_2O_3 were mixed in a quartz cuvette. After 0.5 mL of ice-cold 0.10 M $NaBH_4$ in H_2O was added to the cuvette, the sample was immediately analyzed by UV−vis spectroscopy to obtain the initial concentration of 4-nitrophenolate, and the progress of the reaction was monitored at 2 min time intervals.

RESULTS AND DISCUSSION

$Au_{25}(SC_{10}H_{20}COOH)_{18}$ [$Au_{25}(MUA)_{18}$] and $Au_{25}(SC_{12}H_{25})_{18}$ [$Au_{25}(DDT)_{18}$] clusters were synthesized according to the aforementioned procedures.[26,27] The formation of Au_{25} clusters was verified by UV−vis spectra (Figure S1), which showed three peaks at 399, 446, and 680 nm that are characteristic of molecular transitions of the Au_{25} clusters.[30] We previously reported the matrix-assisted laser desorption/ionization time-of-flight (MALDI-TOF) spectra of such $Au_{25}(MUA)_{18}$ clusters, which gave further evidence for the assignment of $Au_{25}(MUA)_{18}$) clusters.[26] TEM images of the as-synthesized $Au_{25}(MUA)_{18}/Al_2O_3$ and $Au_{25}(DDT)_{18}/Al_2O_3$ before and after ALD are shown in Figure 1. The average

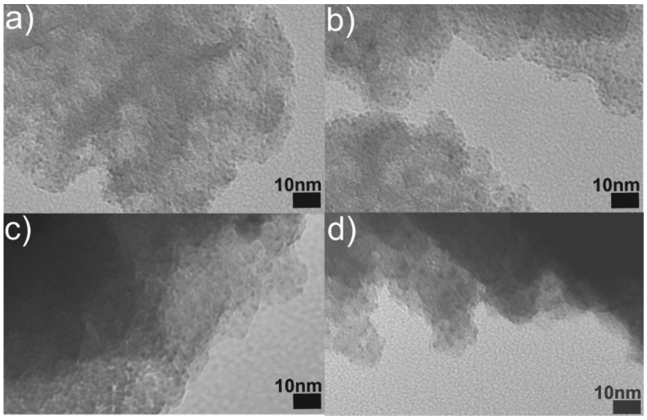

Figure 1. TEM images of as-synthesized (a) $Au_{25}(MUA)_{18}/Al_2O_3$, (b) $Au_{25}(DDT)_{18}/Al_2O_3$, (c) 10c-$Al_2O_3/Au_{25}(MUA)_{18}/Al_2O_3$, and (d) 10c-$Al_2O_3/Au_{25}(DDT)_{18}/Al_2O_3$.

particle sizes of the $Au_{25}(MUA)_{18}/Al_2O_3$ and $Au_{25}(DDT)_{18}/Al_2O_3$ materials were measured to be 1.4 ± 0.1 and 1.5 ± 0.1 nm, respectively. The average particle size of both samples was retained after 10 cycles of alumina deposition. The particle sizes in these samples are slightly larger than the sizes of the pristine clusters deposited on carbon films (∼1.1 nm); the slight size increase is likely an artifact due to imperfect focusing of all clusters in the 3D materials.

Overlayers of alumina were grown onto the $Au_{25}(MUA)_{18}/Al_2O_3$ and $Au_{25}(DDT)_{18}/Al_2O_3$ materials by ALD using sequential pulses of TMA and H_2O. The Au particle sizes of alumina-overcoated samples of $Au_{25}(MUA)_{18}$ clusters with 5, 10, and 20 alumina ALD cycles, followed by calcination, were examined by TEM analysis; the results are shown in Figure 2.

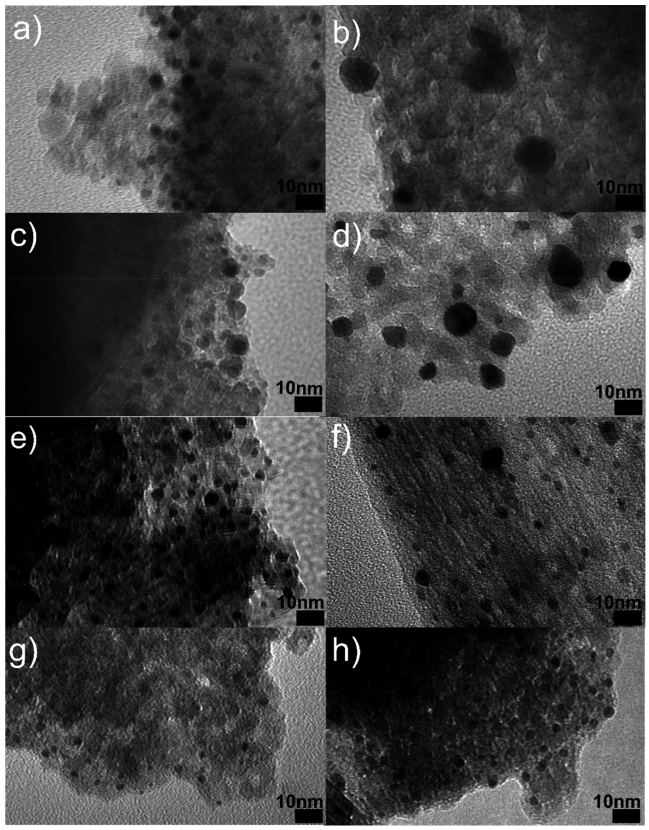

Figure 2. TEM images of $Au_{25}(MUA)_{18}$ samples on Al_2O_3 calcined at (a) 250 and (b) 650 °C, 5c-$Al_2O_3/Au(MUA)/Al_2O_3$ calcined at (c) 250 and (d) 650 °C, 10c-$Al_2O_3/Au(MUA)/Al_2O_3$ calcined at (e) 250 and (f) 650 °C, and 20c-$Al_2O_3/Au(MUA)/Al_2O_3$ calcined at (g) 250 and (h) 650 °C.

Previous work by our group, and others, showed that the thiolate ligands in such clusters are not removed until temperatures of ca. 125 °C and typically completely removed by 250 °C.[7,31] The $Au(MUA)/Al_2O_3$, 5c-$Al_2O_3/Au(MUA)/Al_2O_3$, 10c-$Al_2O_3/Au(MUA)/Al_2O_3$, and 20c-$Al_2O_3/Au(MUA)/Al_2O_3$ catalysts calcined at 250 °C showed average particle sizes of 7.1 ± 6.0, 2.5 ± 1.0, 1.9 ± 0.8, and 1.8 ± 0.8 nm, respectively. Thus, some growth of the clusters via sintering already occurred at this stage, albeit sintering was mitigated with more cycles of alumina deposition. The $Au(MUA)/Al_2O_3$, 5c-$Al_2O_3/Au(MUA)/Al_2O_3$, 10c-$Al_2O_3/Au(MUA)/Al_2O_3$, and 20c-$Al_2O_3/Au(MUA)/Al_2O_3$ samples calcined at 650 °C showed average particle sizes of 11.7 ± 4.0, 6.8 ± 2.8, 2.7 ± 1.6, and 2.4 ± 0.9 nm, respectively. This shows that thicker alumina overcoatings can drastically mitigate sintering at higher temperatures. Prior literature suggests that the coatings would only be 1.1 and 2.2 nm thick for 10- and 20-cycle alumina ALD coatings.[32] We note that we were not able to reproducibly image alumina overcoatings over all of the particles, which is likely due to the lack of contrast between the overcoating and support, although some particles exhibit coatings in the expected size range (Figure S2). Particle-size histograms of each of the samples are shown in

DOI: 10.1021/acsanm.8b01709
ACS Appl. Nano Mater. 2018, 1, 6904−6911

Figure 3. The 10c-Al_2O_3/Au(MUA)/Al_2O_3 and 20c-Al_2O_3/Au(MUA)/Al_2O_3 catalysts exhibited tremendous sinter resistance upon calcination in air up to 650 °C.

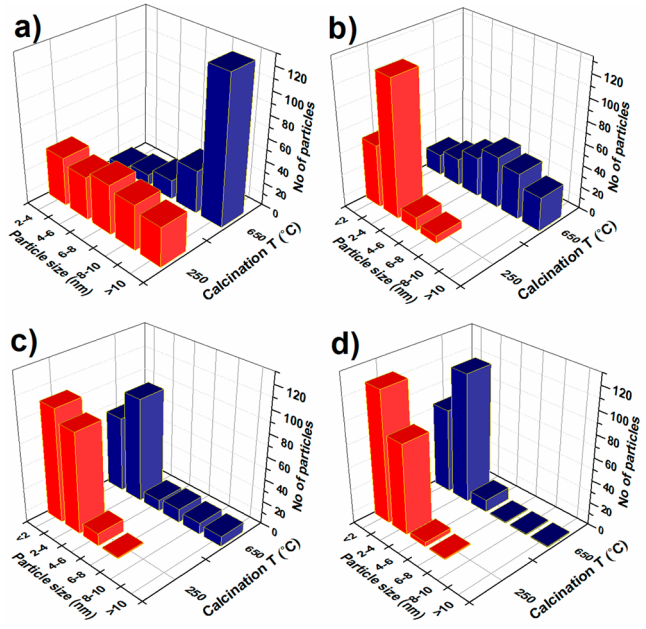

Figure 3. Histograms of (a) Au(MUA)/Al_2O_3, (b) 5c-Al_2O_3/Au(MUA)/Al_2O_3, (c) 10c-Al_2O_3/Au(MUA)/Al_2O_3, and (d) 20c-Al_2O_3/Au(MUA)/Al_2O_3 catalysts calcined at different temperatures.

We also wanted to understand how important the surface chemistry of the clusters was for effective ALD. Thus, we also examined the thermal stability of 10c-Al_2O_3/$Au_{25}(DDT)_{18}$/Al_2O_3 materials; TEM images of the resulting materials after calcination at 250 and 650 °C are shown in Figure 4. The

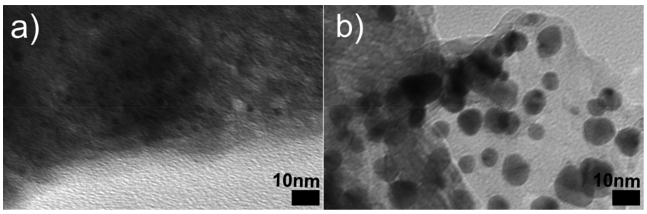

Figure 4. TEM images of 10c-Al_2O_3/$Au_{25}(DDT)_{18}$/Al_2O_3 calcined at (a) 250 and (b) 650 °C.

average particle size increased to 2.0 ± 0.8 nm after calcination at 250 °C and to 5.2 ± 2.1 nm upon calcination at 650 °C. These values are higher than the values seen for comparable $Au_{25}(MUA)_{18}$ samples above (1.9 ± 0.8 and 2.7 ± 1.6 nm for samples calcined at 250 and 650 °C, respectively), particularly for the sample calcined at higher temperature. This implies that that insufficient alumina deposition over $Au_{25}(DDT)_{18}$ clusters occurs, likely because of the lack of functional groups available for anchoring TMA on the DDT ligands.[33] The moderate stability of the $Au_{25}(DDT)_{18}$ system at 250 °C may be explained by alumina growth around the clusters, thus preventing mild sintering at lower temperatures and partially mitigating sintering at higher temperatures (compared to uncoated samples). In the $Au_{25}(MUA)_{18}$ system, on the other hand, the carboxyl groups on the surface of the clusters can allow for anchoring of an alumina overlayer, as shown in Scheme 1; indeed, there is precedence in the literature for growing metal oxide films on the surface of carboxylic acid-terminated self-assembled monolayers.[34,35] First TMA can react with a surface carboxylic acid group to form COO−$Al(CH_3)_2$* and CH_4. Next H_2O is introduced into the reaction chamber and reacts with −$Al((CH)_3)_2$ to form −$Al(OH)_2$* and CH_4. This process is then repeated in the next cycle. It is not clear whether this overlayer on $Au_{25}(MUA)_{18}$ clusters remains completely intact upon removal of the organic thiolate linker in this case; however, the results unambiguously show that much greater sinter resistance is gained in the $Au_{25}(MUA)_{18}$ system compared to the $Au_{25}(DDT)_{18}$ system.

To further understand the effects of 10- and 20-cycle coating on sintering, the $Au_{25}(MUA)_{18}$ samples were also examined by Au L_3-edge EXAFS spectroscopy in fluoresence mode on the hard X-ray microanalysis beamline (HXMA) at the CLS. Figure S3 shows the Au L_3-edge *k*-space and individual *R*-space spectra of the as-synthesized $Au_{25}(MUA)_{18}$ samples coated with 20 layers of alumina prior to calcination. X-ray crystallographic data of $Au_{25}(SR)_{18}$ clusters have shown that $Au_{25}(SR)_{18}$ clusters have a core−shell morphology, where the core is composed of an icosahedral Au_{13} cluster, in which the central atom is surrounded by 12 Au atoms, while the shell consists of six S−Au−S−Au−S staple motifs.[30,36,37] A total of 12 out of the 20 faces of the icosahedron are surrounded by six staple motifs, with S atoms directly attached to 12 Au atoms of the icosahedron core. A multishell fitting approach was used to fit the Au−S and three Au−Au contributions of the clusters in the as-synthesized materials.[31,38] After fitting the parameters for Au−S contribution, we fixed those values, followed by fitting all three first-shell Au−Au coordination modes. CN values for all Au−Au first-shell contributions were fixed based on the crystal structure of the clusters. The final EXAFS fitting parameters are shown in Table S1. The Au−S bond length was found to be 2.32(1) Å, which matches well with the crystallographic data of $Au_{25}L_{18}$ clusters (L = phenylethanethiol). A *R* value at 2.82(3) Å represents the distance between the central Au atom and the surface Au atom of the icosahedron core, whereas 3.03(4) Å is the bond distance between the 12 surface Au atoms of the icosahedron [Au−Au(surf)]. The last Au−Au bond length, 3.31(9) Å, represents the distance between the surface Au atoms and the staple Au atoms. These values are in good agreement with literature values for other Au clusters, and thus the EXAFS data fitting clearly shows that the basic core structures of the Au_{25}(11-MUA)$_{18}$ clusters are retained in the ALD-coated samples prior to calcination.

The Fourier-transformed *R*-space spectra for the 10c-Al_2O_3/Au(MUA)/Al_2O_3 and 20c-Al_2O_3/Au(MUA)/Al_2O_3 samples after calcination at 250 and 650 °C are shown in Figure 5. Individual *k*- and *R*-space spectra of the 10c-Al_2O_3/Au-(MUA)/Al_2O_3, and 20c-Al_2O_3/Au(MUA)/Al_2O_3 samples calcined at two different temperatures, 250 and 650 °C, are shown in Figures S4 and S5, respectively. The Au−S contribution was not observed at 2.3 Å in calcined samples, which suggests that the thiolate ligand is completely removed from the Au surface by 250 °C, which agrees with previous findings by our group and others.[7,15,39] A face-centered-cubic Au model was for used for a single-shell fitting of the calcined samples.[31] Fitted EXAFS parameters of all of the samples are shown in Table 1. In the case of 250 °C-treated 10c-Al_2O_3/Au(MUA)/Al_2O_3 catalysts, the first-shell CN for the Au−Au (N_{Au-Au}) contribution was found to be 10.4(5), which

DOI: 10.1021/acsanm.8b01709
ACS Appl. Nano Mater. 2018, 1, 6904−6911

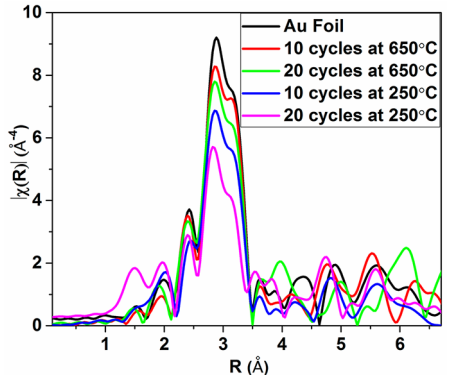

Figure 5. Au L_3-edge EXAFS spectra in the *R* space of the 10c-Al_2O_3/Au(MUA)/Al_2O_3 and 20c-Al_2O_3/Au(MUA)/Al_2O_3 catalysts calcined at different temperatures.

Table 1. EXAFS Fitting Parameters of 10c-Al_2O_3/Au(MUA)/Al_2O_3 and 20c-Al_2O_3/Au(MUA)/Al_2O_3 Materials Calcined at Two Different Temperatures

catalyst	CN(Au–Au)	*R*(Au–Au)/Å	σ^2/Å^2	E_0 shift (eV)
10c-Al_2O_3/Au(MUA)/Al_2O_3 calcined at 250 °C	10.4(5)	2.851(6)	0.0092(9)	4.7(6)
10c-Al_2O_3/Au(MUA)/Al_2O_3 calcined at 650 °C	11.6(5)	2.852(6)	0.0092(7)	3.4(5)
20c-Al_2O_3/Au(MUA)/Al_2O_3 calcined at 250 °C	10.2(5)	2.838(7)	0.010(1)	3.6(6)
20c-Al_2O_3/Au(MUA)/Al_2O_3 calcined at 650 °C	10.5(3)	2.847(4)	0.0081(6)	4.1(4)

increased to 11.6(5) after calcination at 650 °C. The average first-shell CN of 11.6 (compared with 12 for bulk Au) indicates that the average Au particles consist of 10000 or more atoms with an average particle size of 10 nm.[40−43] Because this is significantly larger than the average size seen by TEM, it suggests there are some much larger Au particles in the sample that local TEM analyses do not capture. The first-shell CNs for the Au−Au (N_{Au-Au}) contribution of 20c-Al_2O_3/Au/Al_2O_3 catalysts calcined at 250 and 650 °C were found to be 10.2(5) and 10.5(3), respectively. An average CN of 10.5(3) implies an average particle size of about 2.5−3 nm (containing ∼1600 atoms).[40−43] This value is in reasonable agreement with the TEM data; both TEM and EXAFS studies indicate that catalysts with 20 cycles of alumina deposition showed better sinter resistance than those with 10 cycles of alumina coating.

Previously, we reported that $Au_{25}(MUA)_{18}$ clusters coated with 40 nm silica spheres using sol−gel chemistry also enhanced the thermal stability of $Au_{25}(MUA)_{18}$ clusters and showed a similar average CN of 10.5(6) upon calcination at 650 °C, whereas $Au_{25}(MUA)_{18}$ clusters on silica spheres were not thermally stable and the average particle size increased to 5.1 ± 3.2 nm after calcination at 650 °C.[15] Similarly, Chen et al. found that $Au_{25}[SC_3H_6Si(OCH_3)_3]_{18}$ clusters embedded in a thick silica matrix were found to undergo moderate sintering at 600 °C, and the cluster size increased to 2.2 ± 0.5 nm.[44] The ALD results here show that similar stabilization can be gained with much thinner alumina ALD overlayers. Nakayama et al. investigated the thermal stability of Au_9 clusters on ALD-fabricated amorphous titania with surface roughness measurements. It was found that the height distribution (AFM image) for Au_9 clusters increased from 1.7 ± 0.6 to 2.9 ± 1.6 nm after heat treatment at 200 °C under vacuum (10^{-4} mbar) for 20 min.[45] This reinforces the advantage of having carboxylic acid groups on the surface available for ALD overlayer growth.

To probe the effect of ALD alumina overcoats on the catalytic performance of the resulting materials, we carried out PNP reduction reactions over Au(MUA)/Al_2O_3, 10c-Al_2O_3/

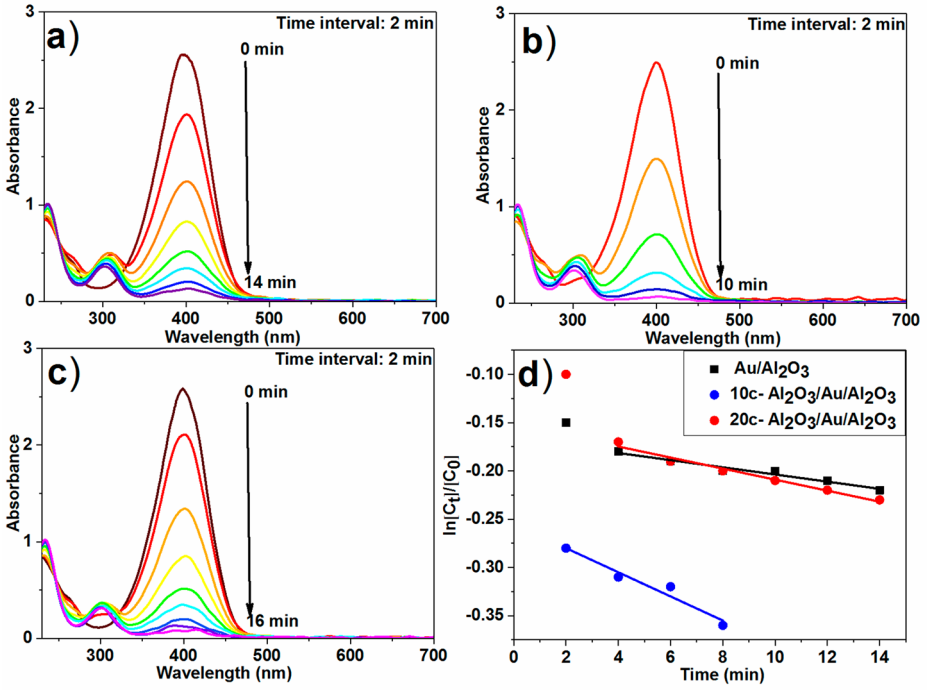

Figure 6. PNP reduction reaction over catalysts calcined at 250 °C: (a) Au(MUA)/Al_2O_3; (b) 10c-Al_2O_3/Au(MUA)/Al_2O_3; (c) 20c-Al_2O_3/Au(MUA)/Al_2O_3. (d) Plot of $\ln(C_t/C_0)$ as a function of the reaction time in minutes.

DOI: 10.1021/acsanm.8b01709
ACS Appl. Nano Mater. 2018, 1, 6904−6911

$Au(MUA)/Al_2O_3$, and $20c\text{-}Al_2O_3/Au(MUA)/Al_2O_3$ catalysts calcined at 250 °C. The PNP reduction results are shown in Figure 6. PNP reduction has been shown by our group and others to be an effective model catalytic reaction to probe the available surface area of Au catalysts.[27,46] After the $NaBH_4$ reducting agent was first added, the PNP solution showed a peak at 400 nm, which corresponds to the nitrophenolate anion.[47−49] The intensity of this peak decreased as a function of time, and a new peak appeared at 300 nm, which corresponded to formation of the 4-aminophenol product.[49] In the absence of Au cluster catalysts, no activity for PNP reduction was observed. The rate constant for the reaction was calculated using pseudo-first-order kinetics; the fits for each of the plots are shown in Figure 6d, and values are shown in Table 2.[50−52] Several samples showed small delay times before catalytic reactions began, which is likely due to the presence of small amounts of oxygen in the system.[53] $10c\text{-}Al_2O_3/Au(MUA)/Al_2O_3$ and $20c\text{-}Al_2O_3/Au(MUA)/Al_2O_3$ catalysts calcined at 250 °C have rate constants of 1.25×10^{-2} and 5.71×10^{-3} min^{-1}, respectively, for nitrophenol reduction. The 20-cycle ALD catalyst showed lower activity, although still slightly higher than that of the uncoated catalyst (3.70×10^{-3} min^{-1}). This drop in the catalytic activity from 10 to 20 cycles of ALD overcoating is not due to the size differences of the particles but rather is likely due to the mass-transfer resistance related to the alumina overlayer.[24] Previous quartz crystal microbalance studies demonstrated that ∼1 Å alumina deposition occurred per cycle;[32,54] thus on the basis of these studies, the $20c\text{-}Al_2O_3/Au(MUA)/Al_2O_3$ catalysts have a 1 nm greater alumina thickness than the $10c\text{-}Al_2O_3/Au(MUA)/Al_2O_3$ catalysts. The rate constants for PNP reduction reaction over $Au(MUA)/Al_2O_3$, $10c\text{-}Al_2O_3/Au(MUA)/Al_2O_3$, and $20c\text{-}Al_2O_3/Au(MUA)/Al_2O_3$ catalysts calcined at 650 °C were 7.19×10^{-4}, 4.49×10^{-4}, and 3.32×10^{-3} min^{-1}, respectively (Figure 7). It is clear that $20c\text{-}Al_2O_3/Au(MUA)/Al_2O_3$ catalysts calcined at 650 °C are more catalytically active than the other two systems, which is likely due to the much smaller particle sizes seen in these samples, as evidenced from EXAFS and TEM analyses. To further analyze the stability of the Au catalysts, $10c\text{-}Al_2O_3/Au(MUA)/Al_2O_3$ and $20c\text{-}Al_2O_3/Au(MUA)/Al_2O_3$ catalysts (calcined at 250 °C) were analyzed by TEM after reaction (Figure S6), and no change in the average Au nanoparticle size was observed after the PNP reduction reaction.

Table 2. Rate Constant k (min^{-1}) for the PNP Reduction Reaction

catalyst	k (min^{-1})	R^2 value
$Au(MUA)/Al_2O_3$ calcined at 250 °C	$3.70 \times 10^{-3} \pm 0.0003$	0.99
$10c\text{-}Al_2O_3/Au(MUA)/Al_2O_3$ calcined at 250 °C	$1.25 \times 10^{-2} \pm 0.001$	0.99
$20c\text{-}Al_2O_3/Au(MUA)/Al_2O_3$ calcined at 250 °C	$5.71 \times 10^{-3} \pm 0.0004$	0.98
$Au(MUA)/Al_2O_3$ calcined at 650 °C	$7.19 \times 10^{-4} \pm 0.0001$	0.95
$10c\text{-}Al_2O_3/Au(MUA)/Al_2O_3$ calcined at 650 °C	$4.49 \times 10^{-4} \pm 0.0001$	0.85
$20c\text{-}Al_2O_3/Au(MUA)/Al_2O_3$ calcined at 650 °C	$3.32 \times 10^{-3} \pm 0.0003$	0.92

CONCLUSIONS

ALD-alumina-overcoated $Au_{25}(MUA)_{18}/Al_2O_3$ samples were synthesized using 5, 10, and 20 cycles of TMA/H_2O exposure. On the basis of TEM and EXAFS analyses, 10 and 20 cycles of alumina overcoating led to improved stability toward sintering compared with uncoated catalysts, with 20 cycles of ALD of alumina dramatically improving the sinter resistance of the Au clusters at high temperatures. 10-cycle alumina ALD coatings

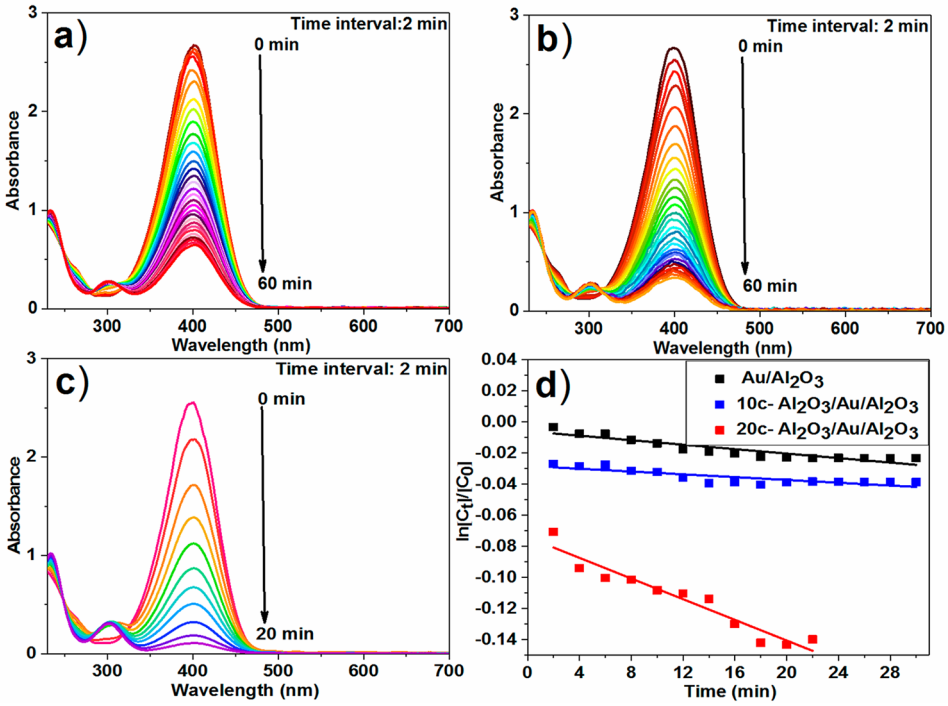

Figure 7. PNP reduction reaction over catalysts calcined at 650°C: (a) $Au(MUA)/Al_2O_3$; (b) $10c\text{-}Al_2O_3/Au(MUA)/Al_2O_3$; (c) $20c\text{-}Al_2O_3/Au(MUA)/Al_2O_3$. (d) Plot of $\ln(C_t/C_0)$ as a function of the reaction time in minutes.

DOI: 10.1021/acsanm.8b01709
ACS Appl. Nano Mater. 2018, 1, 6904−6911

of analogous $Au_{25}(DDT)_{18}$ clusters were less stable to sintering at higher temperatures, likely because alumina coatings could only form around such clusters, while alumina coatings could form on top of the Au_{25}(MUA) samples. PNP reduction reactions carried out over noncoated and 10- and 20-cycle overcoated catalysts showed the highest rate constants for samples with 10 cycles of alumina deposition calcined at 250 °C; however, samples with 20 cycles of alumina deposition were much more effective catalysts after calciantion at 650 °C. These results show that ALD overcoating onto mercaptoalkanoic thiolate stabilizers can be an effective method to stabilize Au clusters from excessive sintering. The resulting supported Au nanoparticle samples should be promising catalysts for a wide range of catalytic processes.

■ ASSOCIATED CONTENT

Supporting Information

The Supporting Information is available free of charge on the ACS Publications website at DOI: 10.1021/acsanm.8b01709.

UV−vis spectra of $Au_{25}L_{18}$ clusters, TEM images of overlayers and spent catalysts, and EXAFS spectral fits and fitting model details for nitrophenol reduction (PDF)

■ AUTHOR INFORMATION

Corresponding Author

*E-mail: robert.scott@usask.ca.

ORCID

Xueliang Sun: 0000-0003-2881-8237

Robert W. J. Scott: 0000-0003-2155-7652

Present Address

§A.L.: Arradiance, 142 North Road, Suite F-150, Sudbury, MA 01776.

Author Contributions

All authors have given approval to the final version of the manuscript. V.S. and R.W.J.S. contributed to the initial concept development, experimental design, characterization of the catalysts, analysis of the results, and writing of the manuscript. ALD work was done in the laboratory of X.S. and carried out by A.L.

Notes

The authors declare no competing financial interest.

■ ACKNOWLEDGMENTS

We acknowledge the National Sciences and Engineering Research Council of Canada (NSERC) for financial support. We thank Ning Chen at the CLS for assistance with XAS measurements. EXAFS experiments described in this paper were performed at the CLS, which is supported by the NSERC, the National Research Council Canada, the Canadian Institutes of Health Research, the Province of Saskatchewan, Western Economic Diversification Canada, and the University of Saskatchewan.

■ REFERENCES

(1) Bharadwaj, S. S.; Schmidt, L. D. Catalytic Partial Oxidation of Natural Gas to Syngas. *Fuel Process. Technol.* **1995**, *42*, 109−127.

(2) Ueda, A.; Oshima, T.; Haruta, M. Reduction of Nitrogen Monoxide with Propene in the Presence of Oxygen and Moisture over Gold Supported on Metal Oxides. *Appl. Catal., B* **1997**, *12*, 81−93.

(3) Gu, D.; Tseng, J. C.; Weidenthaler, C.; Bongard, H. J.; Spliethoff, B.; Schmidt, W.; Soulimani, F.; Weckhuysen, B. M.; Schüth, F. Gold on Different Manganese Oxides: Ultra-Low-Temperature CO Oxidation over Colloidal Gold Supported on Bulk-MnO_2 Nanomaterials. *J. Am. Chem. Soc.* **2016**, *138*, 9572−9580.

(4) Yang, C. M.; Kalwei, M.; Schüth, F.; Chao, K. J. Gold Nanoparticles in SBA-15 Showing Catalytic Activity in CO Oxidation. *Appl. Catal., A* **2003**, *254*, 289−296.

(5) Haruta, M. Size- and Support-Dependency in the Catalysis of Gold. *Catal. Today* **1997**, *36*, 153−166.

(6) Valden, M.; Lai, X.; Goodman, D. W. Onset of Catalytic Activity of Gold Clusters on Titania with the Appearance of Nonmetallic Properties. *Science* **1998**, *281*, 1647−1650.

(7) Nie, X.; Qian, H.; Ge, Q.; Xu, H.; Jin, R. CO Oxidation Catalyzed by Oxide-Supported $Au_{25}(SR)_{18}$ Nanoclusters and Identification of Perimeter Sites as Active Centers. *ACS Nano* **2012**, *6*, 6014−6022.

(8) Antonello, S.; Hesari, M.; Polo, F.; Maran, F. Electron Transfer Catalysis with Monolayer Protected Au_{25} Clusters. *Nanoscale* **2012**, *4*, 5333−5342.

(9) Liu, Y.; Tsunoyama, H.; Akita, T.; Tsukuda, T. Efficient and Selective Epoxidation of Styrene with TBHP Catalyzed by Au_{25} Clusters on Hydroxyapatite. *Chem. Commun.* **2010**, *46*, 550−552.

(10) Martin, J. E.; Odinek, J.; Wilcoxon, J. P.; Anderson, R. A.; Provencio, P. Sintering of Alkanethiol-Capped Gold and Platinum Nanoclusters. *J. Phys. Chem. B* **2003**, *107*, 430−434.

(11) Choy, K. L. Chemical Vapour Deposition of Coatings. *Prog. Mater. Sci.* **2003**, *48*, 57−170.

(12) Liu, Y.; Guerrouache, M.; Kebe, S. I.; Carbonnier, B.; Le Droumaguet, B. Gold Nanoparticles-Supported Histamine-Grafted Monolithic Capillaries as Efficient Microreactors for Flow-through Reduction of Nitro-Containing Compounds. *J. Mater. Chem. A* **2017**, *5*, 11805−11814.

(13) Boisselier, E.; Diallo, A. K.; Salmon, L.; Ornelas, C.; Ruiz, J.; Astruc, D. Encapsulation and Stabilization of Gold Nanoparticles with "Click" Polyethyleneglycol Dendrimers. *J. Am. Chem. Soc.* **2010**, *132*, 2729−2742.

(14) Arnal, P. M.; Comotti, M.; Schüth, F. High-Temperature-Stable Catalysts by Hollow Sphere Encapsulation. *Angew. Chem., Int. Ed.* **2006**, *45*, 8224−8227.

(15) Sudheeshkumar, V.; Shivhare, A.; Scott, R. W. J. Synthesis of Sinter-Resistant Au@silica Catalysts Derived from Au_{25} Clusters. *Catal. Sci. Technol.* **2017**, *7*, 272−280.

(16) Mattevi, C.; Kim, H.; Chhowalla, M. A Review of Chemical Vapour Deposition of Graphene on Copper. *J. Mater. Chem.* **2011**, *21*, 3324−3334.

(17) Puurunen, R. L. Surface Chemistry of Atomic Layer Deposition: A Case Study for the Trimethylaluminum/Water Process. *J. Appl. Phys.* **2005**, *97*, 121301.

(18) George, S. M. Atomic Layer Deposition: An Overview. *Chem. Rev.* **2010**, *110*, 111−131.

(19) Knez, M.; Nielsch, K.; Niinisto, L. Synthesis and Surface Engineering of Complex Nanostructures by Atomic Layer Deposition. *Adv. Mater.* **2007**, *19*, 3425−3438.

(20) Groner, M. D.; Fabreguette, F. H.; Elam, J. W.; George, S. M. Low-Temperature Al_2O_3 Atomic Layer Deposition. *Chem. Mater.* **2004**, *16*, 639−645.

(21) Wang, X.; Tabakman, S. M.; Dai, H. Atomic Layer Deposition of Metal Oxides on Pristine and Functionalized Graphene. *J. Am. Chem. Soc.* **2008**, *130*, 8152−8153.

(22) Chen, P.; Mitsui, T.; Farmer, D. B.; Golovchenko, J.; Gordon, R. G.; Branton, D. Atomic Layer Deposition to Fine-Tune the Surface Properties and Diameters of Fabricated Nanopores. *Nano Lett.* **2004**, *4*, 1333−1337.

(23) Ma, Z.; Brown, S.; Howe, J. Y.; Overbury, S. H.; Dai, S. Surface Modification of Au/TiO_2 Catalysts by SiO_2 via Atomic Layer Deposition. *J. Phys. Chem. C* **2008**, *112*, 9448−9457.

DOI: 10.1021/acsanm.8b01709
ACS Appl. Nano Mater. 2018, 1, 6904−6911

(24) Feng, H.; Lu, J.; Stair, P. C.; Elam, J. W. Alumina over-Coating on Pd Nanoparticle Catalysts by Atomic Layer Deposition: Enhanced Stability and Reactivity. *Catal. Lett.* **2011**, *141*, 512−517.
(25) Lu, J.; Fu, B.; Kung, M. C.; Xiao, G.; Elam, J. W.; Kung, H. H.; Stair, P. C. Coking- and Sintering-Resistant Palladium Catalysts Achieved through Atomic Layer Deposition. *Science* **2012**, *335*, 1205−1208.
(26) Shivhare, A.; Wang, L.; Scott, R. W. J. Isolation of Carboxylic Acid-Protected Au_{25} Clusters Using a Borohydride Purification Strategy. *Langmuir* **2015**, *31*, 1835−1841.
(27) Shivhare, A.; Ambrose, S. J.; Zhang, H.; Purves, R. W.; Scott, R. W. J. Stable and Recyclable Au_{25} Clusters for the Reduction of 4-Nitrophenol. *Chem. Commun.* **2013**, *49*, 276−278.
(28) Schneider, C. A.; Rasband, W. S.; Eliceiri, K. W. NIH Image to ImageJ: 25 Years of Image Analysis. *Nat. Methods* **2012**, *9*, 671−675.
(29) Ravel, B.; Newville, M. ATHENA, ARTEMIS, HEPHAESTUS: Data Analysis for X-ray Absorption Spectroscopy Using IFEFFIT. *J. Synchrotron Radiat.* **2005**, *12*, 537−541.
(30) Zhu, M.; Aikens, C. M.; Hollander, F. J.; Schatz, G. C.; Jin, R. Correlating the Crystal Structure of a Thiol-Protected Au_{25} Cluster and Optical Properties. *J. Am. Chem. Soc.* **2008**, *130*, 5883−5885.
(31) Shivhare, A.; Chevrier, D. M.; Purves, R. W.; Scott, R. W. J. Following the Thermal Activation of $Au_{25}(SR)_{18}$ Clusters for Catalysis by X-ray Absorption Spectroscopy. *J. Phys. Chem. C* **2013**, *117*, 20007−20016.
(32) Whitney, A. V.; Elam, J. W.; Zou, S.; Zinovev, A. V.; Stair, P. C.; Schatz, G. C.; Van Duyne, R. P. Localized Surface Plasmon Resonance Nanosensor: A High-Resolution Distance-Dependence Study Using Atomic Layer Deposition. *J. Phys. Chem. B* **2005**, *109*, 20522−20528.
(33) Avila, J. R.; Demarco, E. J.; Emery, J. D.; Farha, O. K.; Pellin, M. J.; Hupp, J. T.; Martinson, A. B. F. Real-Time Observation of Atomic Layer Deposition Inhibition: Metal Oxide Growth on Self Assembled Alkanethiols. *ACS Appl. Mater. Interfaces* **2014**, *6*, 11891−11898.
(34) Li, M.; Dai, M.; Chabal, Y. J. Atomic Layer Deposition of Aluminum Oxide on Carboxylic Acid-Terminated Self-Assembled Monolayers. *Langmuir* **2009**, *25*, 1911−1914.
(35) Lee, B. H.; Lee, K. H.; Im, S.; Sung, M. M. Monolayer-Precision Fabrication of Mixed-Organic−Inorganic Nanohybrid Superlattices for Flexible Electronic Devices. *Org. Electron.* **2008**, *9*, 1146−1153.
(36) Heaven, M. W.; Dass, A.; White, P. S.; Holt, K. M.; Murray, R. W. Crystal Structure of the Gold Nanoparticle $[N(C_8H_{17})_4][Au_{25}(SCH_2CH_2Ph)_{18}]$. *J. Am. Chem. Soc.* **2008**, *130*, 3754−3755.
(37) Dainese, T.; Antonello, S.; Gascón, J. A.; Pan, F.; Perera, N. V.; Ruzzi, M.; Venzo, A.; Zoleo, A.; Rissanen, K.; Maran, F. $Au_{25}(SEt)_{18}$, A Nearly Naked Thiolate-Protected Au_{25} Cluster: Structural Analysis by Single Crystal X-ray Crystallography and Electron Nuclear Double Resonance. *ACS Nano* **2014**, *8*, 3904−3912.
(38) MacDonald, M. A.; Chevrier, D. M.; Zhang, P.; Qian, H.; Jin, R. The Structure and Bonding of $Au_{25}(SR)_{18}$ Nanoclusters from EXAFS: The Interplay of Metallic and Molecular Behavior. *J. Phys. Chem. C* **2011**, *115*, 15282−15287.
(39) Zhu, Y.; Qian, H.; Jin, R. An Atomic-Level Strategy for Unraveling Gold Nanocatalysis from the Perspective of $Au_n(SR)_m$ Nanoclusters. *Chem. - Eur. J.* **2010**, *16*, 11455−11462.
(40) Ramallo-López, J. M.; Requejo, F. G.; Craievich, A. F.; Wei, J.; Avalos-Borja, M.; Iglesia, E. Complementary Methods for Cluster Size Distribution Measurements: Supported Platinum Nanoclusters in Methane Reforming Catalysts. *J. Mol. Catal. A: Chem.* **2005**, *228*, 299−307.
(41) Jentys, A. Estimation of Mean Size and Shape of Small Metal Particles by EXAFS. *Phys. Chem. Chem. Phys.* **1999**, *1*, 4059−4063.
(42) Fritsche, H. G.; Benfield, R. E. Exact Analytical Formulae for Mean Coordination Numbers in Clusters. *Z. Phys. D: At., Mol. Clusters* **1993**, *26*, 15−17.
(43) Benfield, R. E. Mean Coordination Numbers and the Non-metal-Metal Transition in Clusters. *J. Chem. Soc., Faraday Trans.* **1992**, *88*, 1107−1110.
(44) Chen, H.; Liu, C.; Wang, M.; Zhang, C.; Li, G.; Wang, F. Thermally Robust Silica-Enclosed Au_{25} Nanocluster and its Catalysis. *Chin. J. Catal.* **2016**, *37*, 1787−1793.
(45) Al Qahtani, H. S.; Metha, G. F.; Walsh, R. B.; Golovko, V. B.; Andersson, G. G.; Nakayama, T. Aggregation Behavior of Ligand-Protected Au_9 Clusters on Sputtered Atomic Layer Deposition TiO_2. *J. Phys. Chem. C* **2017**, *121*, 10781−10789.
(46) Wunder, S.; Polzer, F.; Lu, Y.; Mei, Y.; Ballauff, M. Kinetic Analysis of Catalytic Reduction of 4-Nitrophenol by Metallic Nanoparticles Immobilized in Spherical Polyelectrolyte Brushes. *J. Phys. Chem. C* **2010**, *114*, 8814−8820.
(47) Yang, H.; Nagai, K.; Abe, T.; Homma, H.; Norimatsu, T.; Ramaraj, R. Enhanced Catalytic Activity of Gold Nanoparticles Doped in a Mesoporous Organic Gel Based on Polymeric Phloroglucinol Carboxylic Acid−Formaldehyde. *ACS Appl. Mater. Interfaces* **2009**, *1*, 1860−1864.
(48) Dong, F.; Guo, W.; Park, S. K.; Ha, C. S. Controlled Synthesis of Novel Cyanopropyl Polysilsesquioxane Hollow Spheres Loaded with Highly Dispersed Au Nanoparticles for Catalytic Applications. *Chem. Commun.* **2012**, *48*, 1108−1110.
(49) Vysakh, A. B.; Babu, C. L.; Vinod, C. P. Demonstration of Synergistic Catalysis in Au@Ni Bimetallic Core−Shell Nanostructures. *J. Phys. Chem. C* **2015**, *119*, 8138−8146.
(50) Deng, Y.; Cai, Y.; Sun, Z.; Liu, J.; Liu, C.; Wei, J.; Li, W.; Liu, C.; Wang, Y.; Zhao, D. Multifunctional Mesoporous Composite Microspheres with Well-Designed Nanostructure: A Highly Integrated Catalyst System. *J. Am. Chem. Soc.* **2010**, *132*, 8466−8473.
(51) Schrinner, M.; Polzer, F.; Mei, Y.; Lu, Y.; Haupt, B.; Ballauff, M.; Göldel, A.; Drechsler, M.; Preussner, J.; Glatzel, U. Mechanism of the Formation of Amorphous Gold Nanoparticles within Spherical Polyelectrolyte Brushes. *Macromol. Chem. Phys.* **2007**, *208*, 1542−1547.
(52) Baruah, B.; Gabriel, G. J.; Akbashev, M. J.; Booher, M. E. Facile Synthesis of Silver Nanoparticles Stabilized by Cationic Polynorbornenes and their Catalytic Activity in 4-Nitrophenol Reduction. *Langmuir* **2013**, *29*, 4225−4234.
(53) Menumerov, E.; Hughes, R. A.; Neretina, S. Catalytic Reduction of 4-Nitrophenol: A Quantitative Assessment of the Role of Dissolved Oxygen in Determining the Induction Time. *Nano Lett.* **2016**, *16*, 7791−7797.
(54) Ott, A. W.; Klaus, J. W.; Johnson, J. M.; George, S. M. Al_2O_3 Thin Film Growth on Si(100) Using Binary Reaction Sequence Chemistry. *Thin Solid Films* **1997**, *292*, 135−144.

DOI: 10.1021/acsanm.8b01709
ACS Appl. Nano Mater. 2018, 1, 6904−6911